mathematics

Article

A Proposed Analytical and Numerical Treatment for the Nonlinear SIR Model via a Hybrid Approach

Abdulrahman B. Albidah

Department of Mathematics, College of Science, Majmaah University, Al-Majmaah 11952, Saudi Arabia; a.albedah@mu.edu.sa

Abstract: This paper re-analyzes the nonlinear Susceptible–Infected–Recovered (SIR) model using a hybrid approach based on the Laplace–Padé technique. The proposed approach is successfully applied to extract several analytic approximations for the infected and recovered individuals. The domains of applicability of such analytic approximations are addressed. In addition, the present results are validated through various comparisons with the Runge–Kutta numerical method. The obtained analytical results agree with the numerical ones for a wide range of numbers of contacts featured in the studied model. The efficiency of the present analysis reveals that it can be implemented to deal with other systems describing real-life phenomena.

Keywords: Laplace; Padé; ordinary differential equation; initial value problem; series solution; exact solution

MSC: 34A34; 34A45

Citation: Albidah, A.B. A Proposed Analytical and Numerical Treatment for the Nonlinear SIR Model via a Hybrid Approach. *Mathematics* **2023**, *11*, 2749. https://doi.org/10.3390/math11122749

Academic Editors: Roman Parovik, Kholmat Mahkambaevich Shadimetov, Abdullo Rakhmonovich Hayotov and Alicia Cordero

Received: 14 May 2023
Revised: 9 June 2023
Accepted: 13 June 2023
Published: 17 June 2023

1. Introduction

Mathematical models of real-life phenomena are often governed by ordinary differential equations (ODEs) or partial differential equations (PDEs). Searching for analytical or numerical solutions for such models requires accurate methods, whether analytical or numerical, for the better interpretation of the involved phenomena. In this context, mathematicians have invented and developed many ways to solve mathematical and physical models. For example, the Adomian decomposition method (ADM) [1–11] is one of the most popular methods which has been widely used during recent decades; the same applies to the homotopy perturbation method (HPM) [12–15], the homotopy analysis method (HAM) [16,17], and the differential transform method (DTM) [18–21]. However, each of these methods has its own advantages, but at the same time has some defects that must be faced and overcome. Although the above-mentioned methods were found effective in solving a considerable number of mathematical/physical models, a massive amount of computational work is sometimes needed to reach the desired accuracy. The major step when applying the ADM is to calculate the Adomian polynomials of the involved nonlinear terms, while the HPM requires an effective canonical form for the equation/system being solved in addition to imposing an auxiliary parameter. Moreover, one of the main difficulties of the HAM lies in the necessity of choosing an effective/accurate initial guess function, according to which the solution is constructed. Therefore, any unfavorable choice of such an initial guess function will give either an inaccurate or divergent solution.

In order to avoid all the aforementioned difficulties, we will present in this study an alternative approach that may be appropriate and direct to solve ODEs. The first step of the suggested approach is mainly based on obtaining a series solution of the governing equation and then deriving the Laplace transform (LT) of this series. The second step is to construct the Padé approximants of the transformed series and then apply the inverse LT as a final step to construct the approximate analytic solution. For this purpose, it is possible to construct different forms of Padé approximants, including diagonal and non-diagonal. Accordingly, different approximations can be constructed for the required analytic solution. The accuracy of our approach can be validated via performing comparisons with other trusted methods, whether analytical or numerical. In addition, the accuracy of the current method can be evaluated, independently, through calculating the residual errors resulting from the substitution of the obtained approximate analytic solution into the governing equation/system.

The nonlinear Susceptible–Infected–Recovered (SIR) model is considered in this paper as a test example. The SIR model has been employed in Refs. [22,23] to study the COVID-19 pandemic, which is still of interest to many researchers worldwide. The SIR model was first established in Ref. [22] by means of the following system of ODEs:

$$\frac{dR}{d\tau} = I(\tau), \tag{1}$$

$$\frac{dI}{d\tau} = \sigma[1 - R(\tau) - I(\tau)]I(\tau) - I(\tau), \tag{2}$$

where $I(t)$ and $R(t)$ are the infected and the recovered individuals, respectively. $S(t)$ represents the susceptible individuals, $S(t) = 1 - R(t) - I(t)$. The parameter σ describes the transmission rate, which is used to estimate the number of contacts between susceptible and infected individuals. The initial conditions (ICs) are

$$R(0) = A, \quad I(0) = B. \tag{3}$$

A summary of the paper is as follows. In Section 2, a power series solution (PSS) for the system (1)–(3) is derived. Section 3 focuses on applying the proposed approach through combining the LT and the Padé approximants. Furthermore, different analytical approximations for $R(\tau)$ and $I(\tau)$ are established in Section 3. Section 4 is devoted to validating the obtained results, where several comparisons with the Runge–Kutta method are conducted. Moreover, the domains of applicability of the current analysis are demonstrated and addressed in Section 4. In addition, the accuracy of our approach is explored and confirmed via residual errors. The paper is concluded in Section 5.

2. The Series Solution

The system of Equations (1) and (2) can be easily reduced to the following second-order nonlinear ODE:

$$\frac{d^2R}{d\tau^2} = (\sigma - 1)\frac{dR}{d\tau} - \sigma\left(R + \frac{dR}{d\tau}\right)\frac{dR}{d\tau}, \tag{4}$$

under the ICs

$$R(0) = A, \quad \frac{dR(0)}{d\tau} = B. \tag{5}$$

Let us search for a power series solution (PSS) of Equations (4) and (5) in the form:

$$R(\tau) = \sum_{n=0}^{\infty} a_n \tau^n. \tag{6}$$

In view of (5) and (6), the terms a_0 and a_1 are A and B, respectively. Furthermore, we have

$$\left(R + \frac{dR}{d\tau}\right)\frac{dR}{d\tau} = \sum_{n=0}^{\infty}\sum_{k=0}^{n}(n-k+1)(a_k + (k+1)a_{k+1})a_{n-k+1}\tau^n. \tag{7}$$

Substituting (6) and (7) into (4) implies

$$a_{n+2} = \frac{(\sigma-1)a_{n+1}}{n+2} - \frac{\sigma}{(n+1)(n+2)}\sum_{k=0}^{n}(n-k+1)(a_k + (k+1)a_{k+1})a_{n-k+1}, \; n \geq 0. \tag{8}$$

Using the initial terms $a_0 = A$ and $a_1 = B$, the coefficients of the series can be generated and are given as

$$a_2 = -\frac{1}{2}B(1+\sigma(B+A-1)), \tag{9}$$

$$a_3 = \frac{1}{6}B(1+\sigma(B+A-1))^2 + \frac{1}{6}\sigma^2 B^2(B+A-1), \tag{10}$$

$$a_4 = -\frac{1}{24}B(1+\sigma(B+A-1))^3 - \frac{1}{6}\sigma^2 B^2(1+\sigma(B+A-1))(B+A-1) - \frac{1}{24}\sigma^3 B^3(B+A-1), \tag{11}$$

$$a_5 = \frac{1}{120}B(1+\sigma(B+A-1))^4 + \frac{11}{120}\sigma^2 B^2(B+A-1) + \frac{1}{120}\sigma^3 B^3(B+A-1) \times [7+11\sigma(B+A-1)] + \frac{1}{120}\sigma^4 B^4(B+A-1), \tag{12}$$

and so on. Employing the above coefficients in Equation (6), we obtain the following PSS for $R(\tau)$:

$$\begin{aligned} R(\tau) = {}& A + B\tau - B(1+\sigma(B+A-1))\frac{\tau^2}{2!} + \left[B(1+\sigma(B+A-1))^2 + \sigma^2 B^2(B+A-1)\right]\frac{\tau^3}{3!} + \\ & \left[-B(1+\sigma(B+A-1))^3 - 4\sigma^2 B^2(1+\sigma(B+A-1))(B+A-1) - \sigma^3 B^3(B+A-1)\right]\frac{\tau^4}{4!} + \\ & [B(1+\sigma(B+A-1))^4 + 11\sigma^2 B^2(B+A-1) + \sigma^3 B^3(B+A-1)[7+11\sigma(B+A-1)] + \\ & \sigma^4 B^4(B+A-1)]\frac{\tau^5}{5!} + \ldots, \end{aligned} \tag{13}$$

while the PSS for $I(\tau)$ can be obtained through differentiating (6) once with respect to τ, which gives

$$I(\tau) = \sum_{n=0}^{\infty}(n+1)a_{n+1}\tau^n. \tag{14}$$

i.e.,

$$\begin{aligned} I(\tau) = {}& B - B(1+\sigma(B+A-1))\tau + \left[B(1+\sigma(B+A-1))^2 + \sigma^2 B^2(B+A-1)\right]\frac{\tau^2}{2!} + \\ & \left[-B(1+\sigma(B+A-1))^3 - 4\sigma^2 B^2(1+\sigma(B+A-1))(B+A-1) - \sigma^3 B^3(B+A-1)\right]\frac{\tau^3}{3!} + \\ & [B(1+\sigma(B+A-1))^4 + 11\sigma^2 B^2(B+A-1) + \sigma^3 B^3(B+A-1)[7+11\sigma(B+A-1)] + \\ & \sigma^4 B^4(B+A-1)]\frac{\tau^4}{4!} + \ldots, \end{aligned} \tag{15}$$

where the terms of the preceding PSS may be increased as needed to ensure the desired accuracy. However, it will be shown later that the PSS has limitations regarding the domain of convergence. Such drawbacks can be overcome by the current approach which is the subject of the next section.

3. The Laplace–Padé Technique

3.1. Approximation for $R(\tau)$

Applying the Laplace transform (LT) to series (6) yields

$$\overline{R}(s) = \frac{a_0}{s} + \frac{a_1}{s^2} + \frac{2a_2}{s^3} + \frac{6a_3}{s^4} + \frac{24a_4}{s^5} + \frac{120a_5}{s^6} + \ldots. \tag{16}$$

Suppose that $s_1 = 1/s$; then,

$$\overline{R}(s_1) = a_0 s_1 + a_1 s_1^2 + 2a_2 s_1^3 + 6a_3 s_1^4 + 24a_4 s_1^5 + 120a_5 s_1^6 + \ldots \tag{17}$$

Constructing Padé [1/1] for the last series gives

$$\overline{R}_{[1/1]}(s_1) = \frac{a_0 s_1}{1 - \frac{a_1}{a_0} s_1}. \tag{18}$$

Reversing the last expression with respect to s, we obtain

$$\overline{R}_{[1/1]}(s) = \frac{a_0}{s - \frac{a_1}{a_0}}. \tag{19}$$

The inversion of $\overline{R}_{[1/1]}(s)$ gives the approximation $R_{[1/1]}(\tau)$ as

$$R_{[1/1]}(\tau) = a_0 e^{\frac{a_1}{a_0}\tau}. \tag{20}$$

The Padé [1/2] for series (17) is

$$\overline{R}_{[1/2]}(s_1) = \frac{a_0 s_1}{1 - q_1 s_1 + q_2 s_1^2}, \tag{21}$$

where

$$q_1 = \frac{a_1}{a_0}, \quad q_2 = \left(\frac{a_1}{a_0}\right)^2 - \frac{2a_2}{a_0}. \tag{22}$$

Equation (21) implies

$$\overline{R}_{[1/2]}(s) = \frac{a_0 s}{s^2 - q_1 s + q_2}, \tag{23}$$

and hence,

$$R_{[1/2]}(\tau) = a_0 e^{\frac{1}{2}q_1\tau}\left[\cosh\left(\frac{1}{2}\sqrt{q_1^2 - 4q_2}\,\tau\right) + \frac{q_1}{\sqrt{q_1^2 - 4q_2}}\sinh\left(\frac{1}{2}\sqrt{q_1^2 - 4q_2}\,\tau\right)\right], \tag{24}$$

provided that

$$q_1^2 - 4q_2 > 0. \tag{25}$$

This expression transforms to the trigonometric form

$$R_{[1/2]}(\tau) = a_0 e^{\frac{1}{2}q_1\tau}\left[\cos\left(\frac{1}{2}\sqrt{4q_2 - q_1^2}\,\tau\right) + \frac{q_1}{\sqrt{4q_2 - q_1^2}}\sin\left(\frac{1}{2}\sqrt{4q_2 - q_1^2}\,\tau\right)\right], \tag{26}$$

when

$$4q_2 - q_1^2 > 0. \tag{27}$$

From (17), we have the following expression for Padé $[2/2](s_1)$:

$$\overline{R}_{[2/2]}(s_1) = \frac{a_0 s_1 + p_1 s_1^2}{1 - r_1 s_1 + r_2 s_1^2}, \tag{28}$$

where

$$p_1 = \frac{a_1^3 - 4a_0 a_1 a_2 + 6a_0^2 a_3}{a_1^2 - 2a_0 a_2}, \quad r_1 = \frac{2(a_1 a_2 - 3a_0 a_3)}{a_1^2 - 2a_0 a_2}, \quad r_2 = \frac{2(2a_2^2 - 3a_1 a_3)}{a_1^2 - 2a_0 a_2}. \tag{29}$$

Based on (28), we have

$$\overline{R}_{[2/2]}(s) = \frac{a_0 s + p_1}{s^2 - r_1 s + r_2}, \tag{30}$$

which leads to

$$R_{[2/2]}(\tau) = e^{\frac{1}{2}r_1\tau}\left[a_0\cosh\left(\frac{1}{2}\sqrt{r_1^2-4r_2}\,\tau\right) + \frac{2p_1+a_0r_1}{\sqrt{r_1^2-4r_2}}\sinh\left(\frac{1}{2}\sqrt{r_1^2-4r_2}\,\tau\right)\right],\ r_1^2-4r_2>0, \tag{31}$$

or equivalently,

$$R_{[2/2]}(\tau) = e^{\frac{1}{2}r_1\tau}\left[a_0\cos\left(\frac{1}{2}\sqrt{4r_2-r_1^2}\,\tau\right) + \frac{2p_1+a_0r_1}{\sqrt{4r_2-r_1^2}}\sin\left(\frac{1}{2}\sqrt{4r_2-r_1^2}\,\tau\right)\right],\ 4r_2-r_1^2>0. \tag{32}$$

Similarly, one can obtain

$$\overline{R}_{[2/3]}(s) = \frac{a_0s^2+u_1s}{s^3-v_1s^2+v_2s+v_3}, \tag{33}$$

which can be inverted to give

$$R_{[2/3]}(\tau) = h_1e^{z_1\tau} + h_2e^{z_2\tau} + h_3e^{z_3\tau}, \tag{34}$$

where the quantities u_1, v_i and h_i $(i=1,2,3)$ are given by

$$u_1 = \frac{a_1^4-6a_0a_1^2a_2+4a_0^2a_2^2+12a_0^2a_1a_3-24a_0^3a_4}{a_1^3-4a_0a_1a_2+6a_0^2a_3}, \tag{35}$$

$$v_1 = \frac{2\left(a_1^2a_2-2a_0a_2^2-3a_0a_1a_3+12a_0^2a_4\right)}{a_1^3-4a_0a_1a_2+6a_0^2a_3}, \tag{36}$$

$$v_2 = \frac{2\left(2a_1a_2^2-3a_1^2a_3-6a_0a_2a_3+12a_0a_1a_4\right)}{a_1^3-4a_0a_1a_2+6a_0^2a_3}, \tag{37}$$

$$v_3 = \frac{4\left(-2a_2^3+6a_1a_2a_3-9a_0a_3^2-6a_1^2a_4+12a_0a_2a_4\right)}{a_1^3-4a_0a_1a_2+6a_0^2a_3}, \tag{38}$$

and

$$h_1 = \frac{a_0z_1^2+u_1z_1}{(z_1-z_2)(z_1-z_3)},\quad h_2 = \frac{a_0z_2^2+u_1z_2}{(z_2-z_1)(z_2-z_3)},\quad h_3 = \frac{a_0z_3^2+u_1z_3}{(z_3-z_1)(z_3-z_2)}. \tag{39}$$

Furthermore, z_1, z_2, and z_3 are three distinct roots of the cubic algebraic equation

$$z^3-v_1z^2+v_2z+v_3=0. \tag{40}$$

Furthermore, we can calculate the diagonal Padé approximant $\overline{R}_{[3/3]}(s)$ as

$$\overline{R}_{[3/3]}(s) = \frac{a_0s^2+w_1s+w_2}{s^3-d_1s^2+d_2s+d_3}, \tag{41}$$

which has the following inversion:

$$R_{[3/3]}(\tau) = l_1e^{m_1\tau} + l_2e^{m_2\tau} + l_3e^{m_3\tau}, \tag{42}$$

where the quantities w_1, w_2, d_i and l_i $(i=1,2,3)$ are

$$w_1 = \frac{2\left(a_1a_2^3 - 3a_1^2a_2a_3 - 3a_0a_2^2a_3 + 9a_0a_1a_3^2 + 3a_1^3a_4 - 18a_0^2a_3a_4 - 15a_0a_1^2a_5 + 30a_0^2a_2a_5\right)}{2a_2^3 - 6a_1a_2a_3 + 9a_0a_3^2 + 6a_1^2a_4 - 12a_0a_2a_4}, \tag{43}$$

$$\begin{aligned} w_2 = {} & (4a_2^4 - 18a_1a_2^2a_3 + 9a_1^2a_3^2 + 36a_0a_2a_3^2 + 24a_1^2a_2a_4 - 48a_0a_2^2a_4 - 72a_0a_1a_3a_4 + 144a_0^2a_4^2 - \\ & 30a_1^3a_5 + 120a_0a_1a_2a_5 - 180a_0^2a_3a_5)\,/\,(2a_2^3 - 6a_1a_2a_3 + 9a_0a_3^2 + 6a_1^2a_4 - 12a_0a_2a_4), \end{aligned} \tag{44}$$

$$d_1 = \frac{3\left(2a_2^2a_3 - 3a_1a_3^2 - 4a_1a_2a_4 + 12a_0a_3a_4 + 10a_1^2a_5 - 20a_0a_2a_5\right)}{2a_2^3 - 6a_1a_2a_3 + 9a_0a_3^2 + 6a_1^2a_4 - 12a_0a_2a_4}, \tag{45}$$

$$d_2 = \frac{6\left(3a_2a_3^2 - 4a_2^2a_4 - 6a_1a_3a_4 + 24a_0a_4^2 + 10a_1a_2a_5 - 30a_0a_3a_5\right)}{2a_2^3 - 6a_1a_2a_3 + 9a_0a_3^2 + 6a_1^2a_4 - 12a_0a_2a_4}, \tag{46}$$

$$d_3 = \frac{6\left(-9a_3^3 + 24a_2a_3a_4 - 24a_1a_4^2 - 20a_2^2a_5 + 30a_1a_3a_5\right)}{2a_2^3 - 6a_1a_2a_3 + 9a_0a_3^2 + 6a_1^2a_4 - 12a_0a_2a_4}, \tag{47}$$

and

$$l_1 = \frac{a_0m_1^2 + w_1m_1 + w_2}{(m_1 - m_2)(m_1 - m_3)}, \quad l_2 = \frac{a_0m_2^2 + w_1m_2 + w_2}{(m_2 - m_1)(m_2 - m_3)}, \quad l_3 = \frac{a_0m_3^2 + w_1m_3 + w_2}{(m_3 - m_1)(m_3 - m_2)}. \tag{48}$$

while m_i, $i = 1, 2, 3$ are three distinct roots of the cubic equation

$$m^3 - d_1m^2 + d_2m + d_3 = 0. \tag{49}$$

Remark 1. *It should be noted that the inversion of Equation (41) depends on the three roots of the denominator. To clarify this point, assume that m_i, $i = 1, 2, 3$ are three distinct roots of the denominator in (41), i.e., $s^3 - d_1s^2 + d_2s + d_3 = (s - m_1)(s - m_2)(s - m_3)$; then, one can rewrite Equation (41) as*

$$\overline{R}_{[3/3]}(s) = \frac{a_0s^2 + w_1s + w_2}{s^3 - d_1s^2 + d_2s + d_3} = \frac{a_0s^2 + w_1s + w_2}{(s - m_1)(s - m_2)(s - m_3)}.$$

Using partial fractions, we can express $\overline{R}_{[3/3]}(s)$ as

$$\overline{R}_{[3/3]}(s) = \frac{l_1}{s - m_1} + \frac{l_2}{s - m_2} + \frac{l_3}{s - m_3},$$

where l_i, $i = 1, 2, 3$ are given by Equation (48). It is now clear that the inversion of $\overline{R}_{[3/3]}(s)$ in the last equation gives Formula (42).

3.2. Approximation for $I(\tau)$

Proceeding as above, one can obtain

$$\bar{I}_{[1/1]}(s) = \frac{a_1}{s - \frac{2a_2}{a_1}}, \tag{50}$$

and

$$\bar{I}_{[2/2]}(s) = \frac{a_1s + b_1}{s^2 - c_1s + c_2}. \tag{51}$$

The inversions of the above expressions give

$$I_{[1/1]}(\tau) = a_1e^{\frac{2a_2}{a_1}\tau}, \tag{52}$$

and

$$I_{[2/2]}(\tau) = e^{\frac{1}{2}c_1\tau}\left[a_1\cosh\left(\frac{1}{2}\sqrt{c_1^2 - 4c_2}\,\tau\right) + \frac{2b_1 + a_1c_1}{\sqrt{c_1^2 - 4c_2}}\sinh\left(\frac{1}{2}\sqrt{c_1^2 - 4c_2}\,\tau\right)\right],\ c_1^2 - 4c_2 > 0, \tag{53}$$

where

$$b_1 = \frac{4(a_2^3 - 3a_1a_2a_3 + 3a_1^2a_4)}{2a_2^2 - 3a_1a_3}, \quad c_1 = \frac{6(a_2a_3 - 2a_1a_4)}{2a_2^2 - 3a_1a_3}, \quad c_2 = \frac{6(3a_3^2 - 4a_2a_4)}{2a_2^2 - 3a_1a_3}. \tag{54}$$

The approximation $I_{[3/3]}(\tau)$ can also be established using the same procedure. However, it will be shown later that $I_{[2/2]}(\tau)$ is sufficient to achieve the desired accuracy.

4. Results and Validation

In this section, we focus on validating the accuracy of the current analysis. Various comparisons are performed to reveal the validity of the present PSS and the Padé approximants for the recovered and infected individuals $R(\tau)$ and $I(\tau)$, respectively. The explicit Runge–Kutta method (ERKM) is chosen as a reference numerical method to explore the effectiveness and efficiency of our accuracy.

To achieve this task, we may express the j-term of the PSS for $R(\tau)$ and $I(\tau)$, respectively, as

$$\Phi_j(\tau) = \sum_{n=0}^{j-1} a_n\tau^n, \quad \Psi_j(\tau) = \sum_{n=0}^{j-1} (n+1)a_{n+1}\tau^n. \tag{55}$$

Before launching into the main target of this section, we may shed some light on the domains of applicability/inapplicability for the expressions of $R_{[2/2]}(\tau)$ and $I_{[2/2]}(\tau)$ in Equations (31) and (53), respectively. It can be noted from Figure 1 that the approximation $R_{[2/2]}(\tau)$ is applicable in certain domains for A and B when $\sigma = 0.7$. However, Figure 2 shows that the corresponding approximation $I_{[2/2]}(\tau)$, at $\sigma = 0.7$, is applicable in all possible domains of A and B provided that $A + B = 1$ is not satisfied, i.e., $A + B \neq 1$. Actually, it can be declared that the restriction $A + B = 1$ leads to exact expressions of $R(\tau)$ and $I(\tau)$. In such cases, the PSS (13) reduces to

$$R(\tau) = A + B\left(\tau - \frac{\tau^2}{2!} + \frac{\tau^3}{3!} - \frac{\tau^4}{4!} + \frac{\tau^5}{5!} + \dots\right) = 1 - Be^{-\tau}, \tag{56}$$

while the PSS (15) becomes

$$I(\tau) = B\left(\tau - \frac{\tau^2}{2!} + \frac{\tau^3}{3!} - \frac{\tau^4}{4!} + \frac{\tau^5}{5!} + \dots\right) = Be^{-\tau}. \tag{57}$$

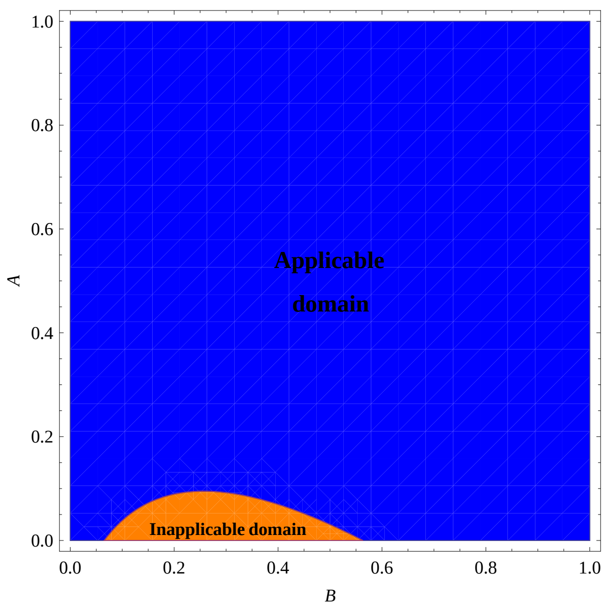

Figure 1. Applicability/inapplicability domains of the $R_{[2/2]}(\tau)$ at $\sigma = 0.7$.

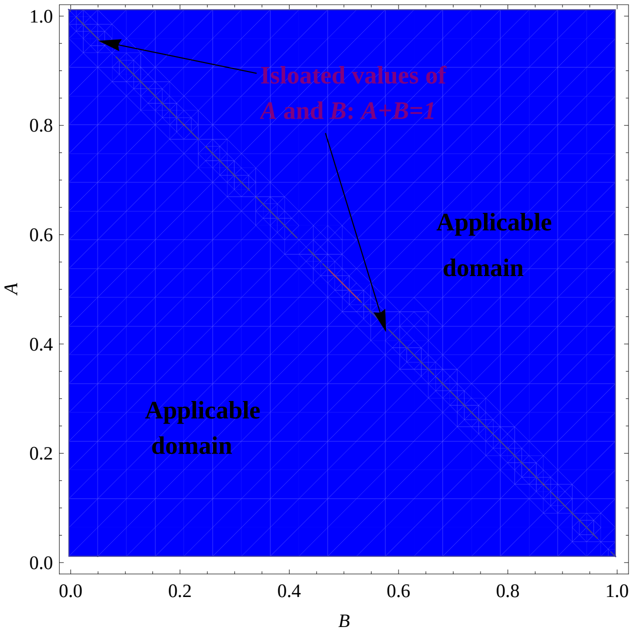

Figure 2. Applicability/inapplicability domains of the $I_{[2/2]}(\tau)$ at $\sigma = 0.7$.

In addition, Figures 3 and 4 show the applicability/inapplicability domains of $R_{[2/2]}(\tau)$ and $I_{[2/2]}(\tau)$ at $\sigma = 0.9$. In Figure 5, the curves of the PSS $\Phi_{10}(\tau)$ and the Padé approximant $R_{[2/2]}(\tau)$ are compared with the numerical solution at $A = 0$, $B = 10^{-3}$, and $\sigma = 0.5$. This figure indicates that the domain of agreement with the numerical solution is increased through $R_{[2/2]}(\tau)$, while the PSS $\Phi_{10}(\tau)$ coincides with the numerical solution in a short domain. Furthermore, Figure 6 confirms this conclusion regarding the Padé approximant $I_{[2/2]}(\tau)$ and the PSS $\Psi_{10}(\tau)$. Similar results can be seen in Figures 7–10. It can be observed from Figure 7 ($\sigma = 0.7$) and Figure 9 ($\sigma = 0.9$) that the difference between the $R_{[2/2]}(\tau)$ and the numerical solution slightly increases at large values of τ but the $R_{[2/2]}(\tau)$ is still better than the PSS $\Phi_{10}(\tau)$.

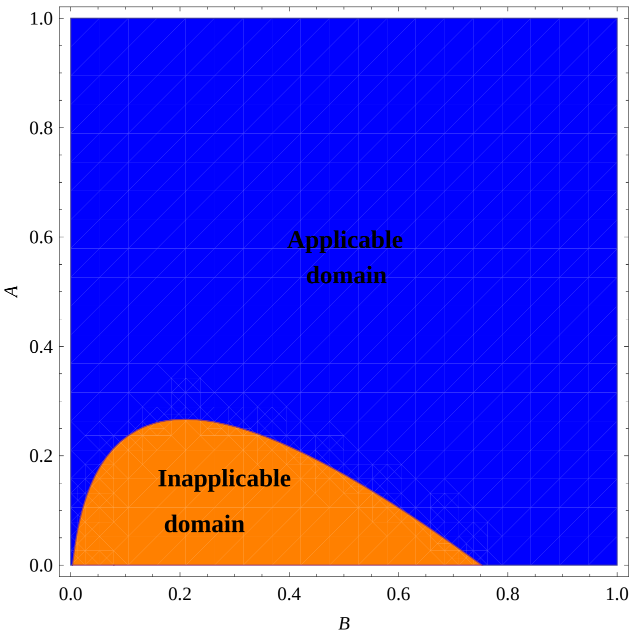

Figure 3. Applicability/inapplicability domains of the $R_{[2/2]}(\tau)$ at $\sigma = 0.9$.

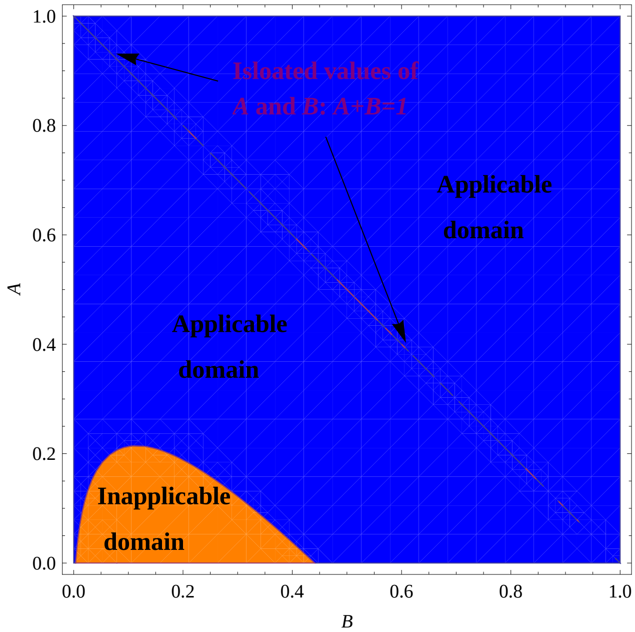

Figure 4. Applicability/inapplicability domains of the $I_{[2/2]}(\tau)$ at $\sigma = 0.9$.

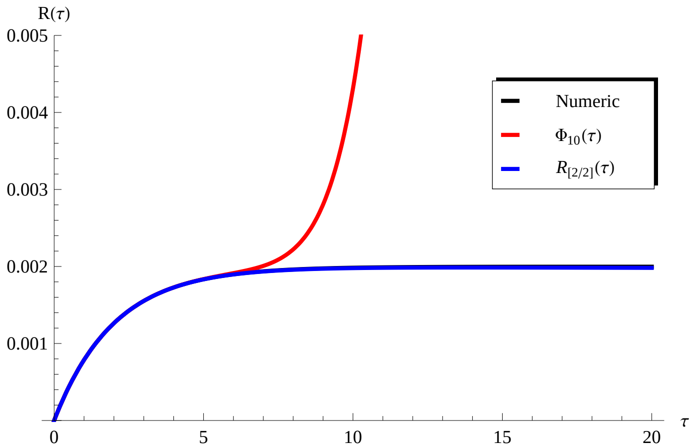

Figure 5. Plots of the PSS $\Phi_{10}(\tau)$, the $R_{[2/2]}(\tau)$, and the numerical solution at $A = 0$, $B = 10^{-3}$, and $\sigma = 0.5$.

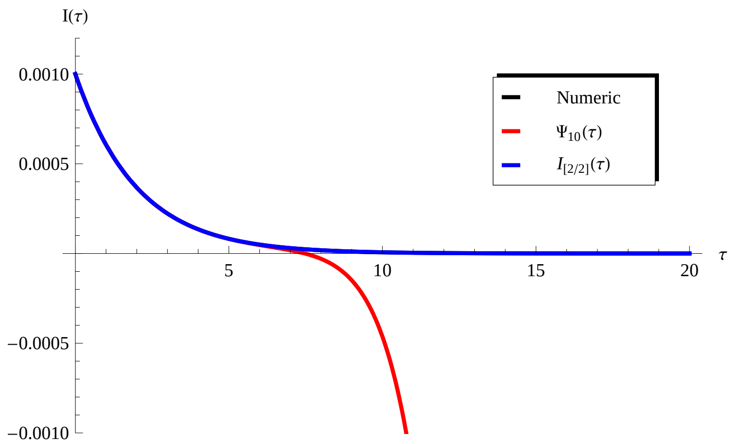

Figure 6. Plots of the PSS $\Psi_{10}(\tau)$, the $I_{[2/2]}(\tau)$, and the numerical solution at $A = 0$, $B = 10^{-3}$, and $\sigma = 0.5$.

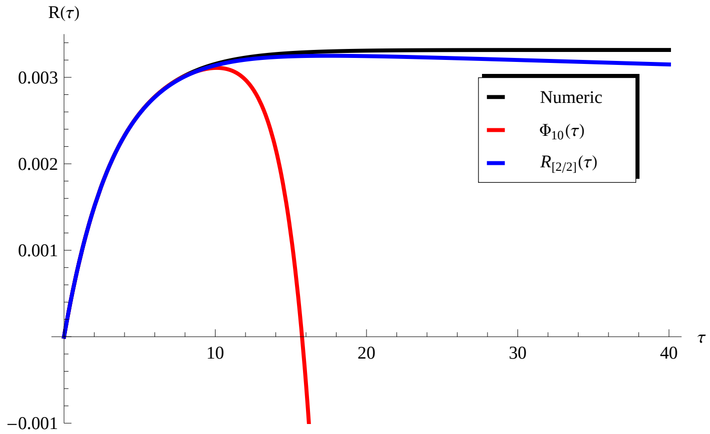

Figure 7. Plots of the PSS $\Phi_{10}(\tau)$, the $R_{[2/2]}(\tau)$, and the numerical solution at $A = 0$, $B = 10^{-3}$, and $\sigma = 0.7$.

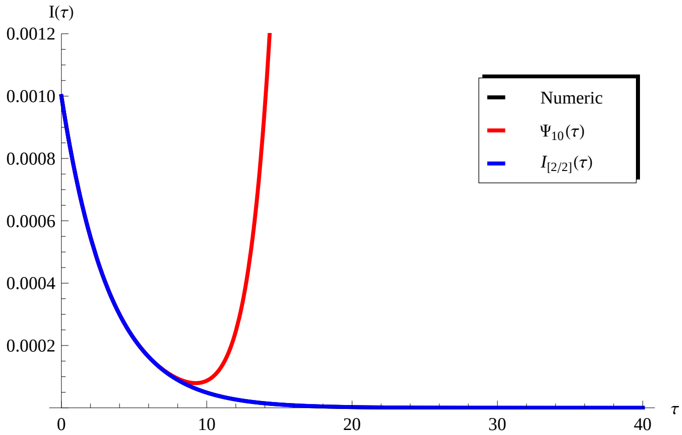

Figure 8. Plots of the PSS $\Psi_{10}(\tau)$, the $I_{[2/2]}(\tau)$, and the numerical solution at $A = 0$, $B = 10^{-3}$, and $\sigma = 0.7$.

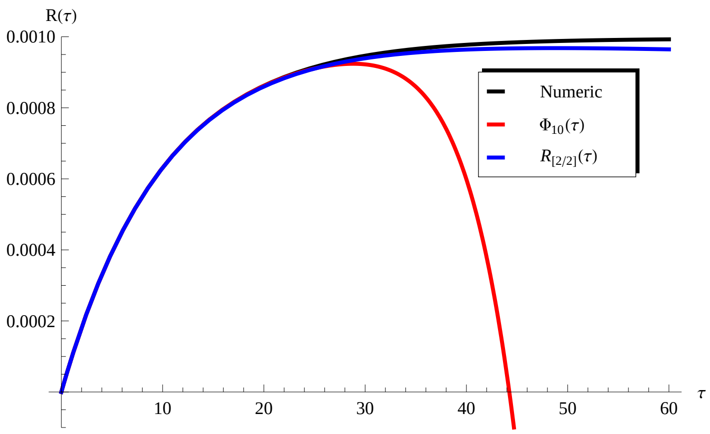

Figure 9. Plots of the PSS $\Phi_{10}(\tau)$, the $R_{[2/2]}(\tau)$, and the numerical solution at $A = 0$, $B = 10^{-4}$, and $\sigma = 0.9$.

Such a limitation can be easily overcome through considering a higher-order Padé approximant, as will be demonstrated later. On the other hand, one can see from Figure 8 ($\sigma = 0.7$) and Figure 10 ($\sigma = 0.9$) that the curves of the $I_{[2/2]}(\tau)$ are in full agreement with the numerical ones in the whole domain of τ. In order overcome the limitations mentioned above, the higher-order Padé approximant $R_{[3/3]}(\tau)$ is depicted in Figures 11 and 12 at

$\sigma = 0.9$ and $\sigma = 0.95$, respectively. It is clear from these figures that the approximation $R_{[3/3]}(\tau)$ agrees with the numerical solution in the whole domain. Moreover, the residual error $RE(\tau)$ for Equations (1) and (2) is depicted in Figures 13 and 14 using the current Padé approximants $R_{[2/2]}$ and $I_{[2/2]}$. Furthermore, numerical comparisons are performed between the present PSS $\Phi_{10}(\tau)$, $\Psi_{10}(\tau)$, $R_{[2/2]}(\tau)$, and the $I_{[2/2]}(\tau)$ with the ERKM in Tables 1 and 2.

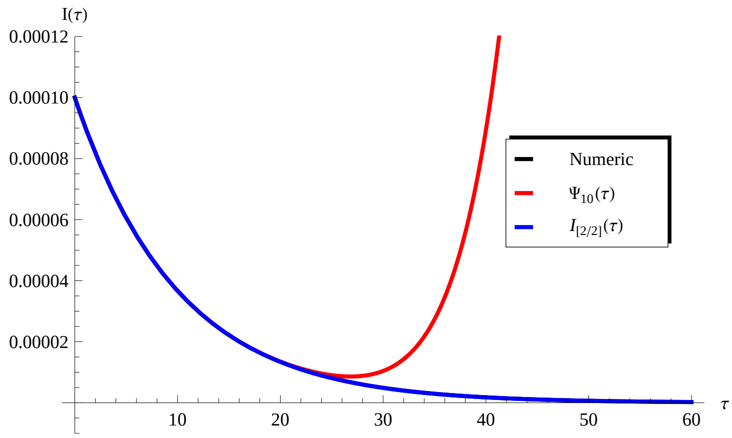

Figure 10. Plots of the PSS $\Psi_{10}(\tau)$, the $I_{[2/2]}(\tau)$, and the numerical solution at $A = 0$, $B = 10^{-4}$, and $\sigma = 0.9$.

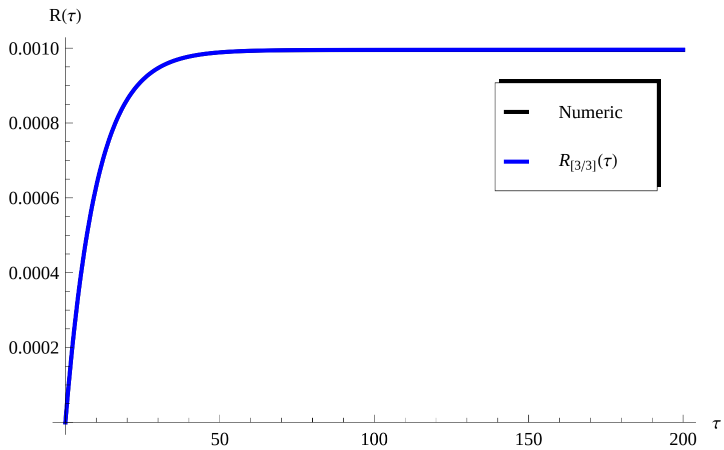

Figure 11. Plots of the $R_{[3/3]}(\tau)$ and the numerical solution at $A = 0$, $B = 10^{-4}$, and $\sigma = 0.9$.

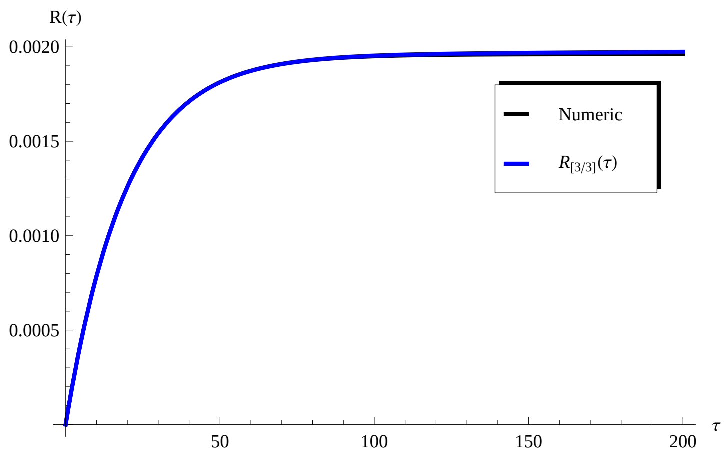

Figure 12. Plots of the $R_{[3/3]}(\tau)$ and the numerical solution at $A = 0$, $B = 10^{-4}$, and $\sigma = 0.95$.

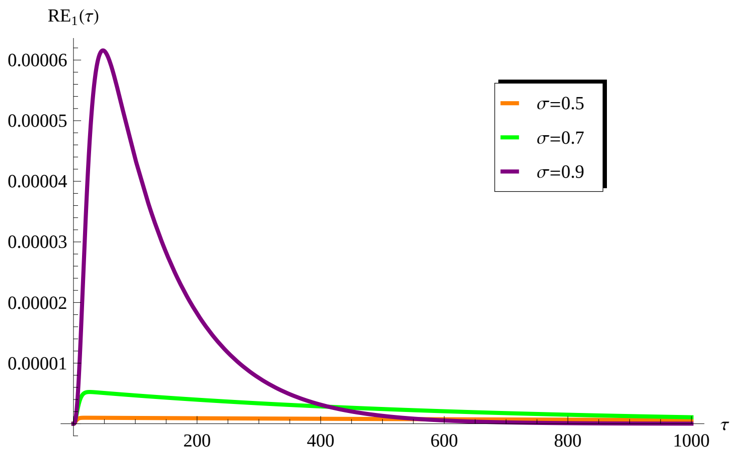

Figure 13. Variation in the residual $RE_1(\tau)$ at various values of σ when $A = 0$ and $B = 10^{-3}$.

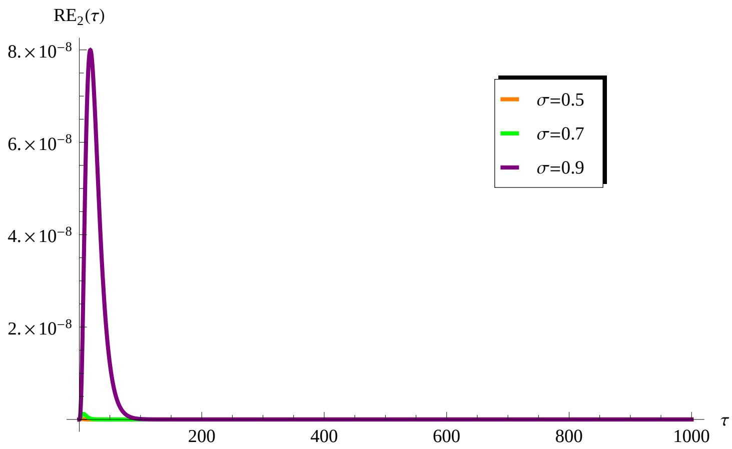

Figure 14. Variation of the residual $RE_2(\tau)$ at various values of σ when $A = 0$ and $B = 10^{-3}$.

Table 1. Comparisons of the present PSS $\Phi_{10}(\tau)$ and the LT-Padé approximant $R_{[2/2]}(\tau)$ with the ERKM at $\sigma = 0.5$, $A = 0$ and $B = 0.001$.

τ	$\Phi_{10}(\tau)$ (Present)	$R_{[2/2]}(\tau)$ (Present)	ERKM (Numerical)
5	0.0018364	0.0018327	0.0018338
10	0.0043093	0.0019785	0.0019837
15	0.1220652	0.0019860	0.0019959
20	1.9188949	0.0019820	0.0019969
25	16.160833	0.0019772	0.0019970
30	91.203779	0.0019722	0.0019970
35	390.97111	0.0019673	0.0019970
40	1372.0035	0.0019624	0.0019970
45	4135.3979	0.0019575	0.0019970
50	11061.598	0.0019526	0.0019970

In order to reveal the effectiveness of the our approach over the homotopy perturbation method (HPM) in the literature [23], we present a comparison between the $R_{[3/3]}(\tau)$ (present), the numerical solution, and the HPM (Ref. [23]) at $\sigma = 0.9$ and $\sigma = 0.95$ in Figures 15 and 16, respectively, when $A = 0$ and $B = 10^{-4}$. These figures show that our solution is closer to the numerical one (nearly identical) when compared with the HPM in Ref. [23].

Table 2. Comparisons of the present PSS $\Psi_{10}(\tau)$ and the LT-Padé approximant $I_{[2/2]}(\tau)$ with the ERKM at $\sigma = 0.5$, $A = 0$ and $B = 0.001$.

τ	$\Psi_{10}(\tau)$ (Present)	$I_{[2/2]}(\tau)$ (Present)	ERKM (Numerical)
5	$+8.1388 \times 10^{-5}$	8.1751×10^{-5}	8.1749×10^{-5}
10	-4.6305×10^{-4}	6.6776×10^{-6}	6.6762×10^{-6}
15	-2.8065×10^{-2}	5.4540×10^{-7}	5.4521×10^{-7}
20	-4.8604×10^{-1}	4.4546×10^{-8}	4.4400×10^{-8}
25	$-0.4315 \times 10^{+1}$	3.6384×10^{-9}	3.6015×10^{-9}
30	$-0.2524 \times 10^{+2}$	2.9717×10^{-10}	2.9778×10^{-10}
35	$-0.1110 \times 10^{+3}$	2.4274×10^{-11}	2.4386×10^{-11}
40	$-0.3975 \times 10^{+3}$	1.9824×10^{-12}	2.5862×10^{-12}
45	$-0.1217 \times 10^{+4}$	1.6491×10^{-13}	1.7257×10^{-13}
50	$-0.3296 \times 10^{+4}$	1.3225×10^{-14}	1.7449×10^{-13}

The above results reveal that the accuracy can be enhanced by applying the current hybrid approach. This is of course one of the main advantages of the proposed method.

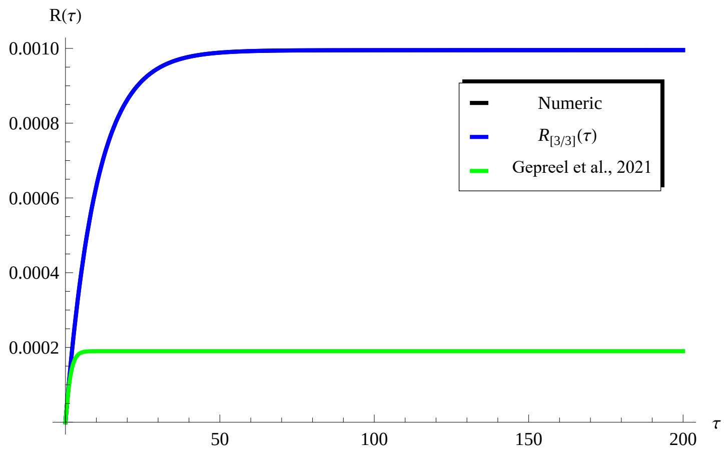

Figure 15. Comparison between the $R_{[3/3]}(\tau)$ (present), the numerical solution, and the HPM (Ref. [23]) at $A = 0$, $B = 10^{-4}$, and $\sigma = 0.9$.

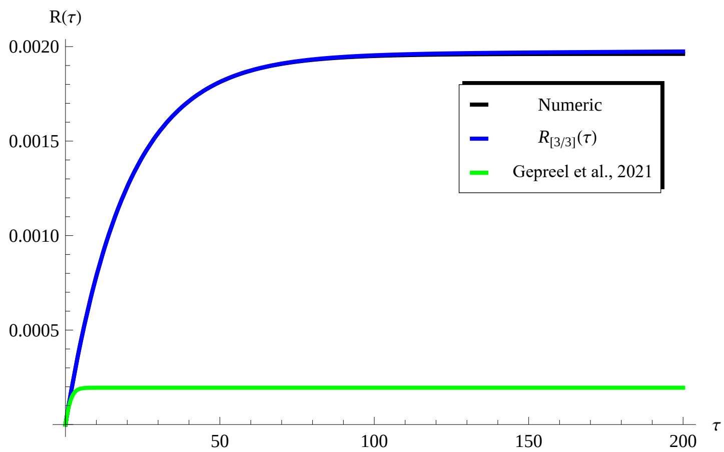

Figure 16. Comparison between the $R_{[3/3]}(\tau)$ (present), the numerical solution, and the HPM (Ref. [23]) at $A = 0$, $B = 10^{-4}$, and $\sigma = 0.95$.

5. Conclusions

In this paper, the nonlinear SIR model was solved using a hybrid approach. The proposed technique was based on combining the LT and the Padé approximants. Various analytic approximations were successfully conducted for the infected and the recovered individuals. Moreover, such analytic approximations were found to be applicable in specific domains, which were described analytically and graphically. The performed comparisons with the explicit Runge–Kutta numerical method reveal the accuracy of the obtained results. Furthermore, the calculated residuals confirm this conclusion. The effectiveness of our approach reveals its ability to treat other mathematical and physical models in the applied sciences.

Funding: The author would like to thank Deanship of Scientific Research at Majmaah University for supporting this work under Project Number No. R-2023-483.

Data Availability Statement: Not applicable.

Acknowledgments: The author also would like to thank the referees for their valuable comments and suggestions which helped to improve the manuscript.

Conflicts of Interest: The author declares that there are no competing interest regarding the publication of this paper.

References

1. Ebaid, A. Approximate analytical solution of a nonlinear boundary value problem and its application in fluid mechanics. *Z. Naturforschung A* **2011**, *66*, 423–426. [CrossRef]
2. Duan, J.S.; Rach, R. A new modification of the Adomian decomposition method for solving boundary value problems for higher order nonlinear differential equations. *Appl. Math. Comput.* **2011**, *218*, 4090–4118. [CrossRef]
3. Ebaid, A. A new analytical and numerical treatment for singular two-point boundary value problems via the Adomian decomposition method. *J. Comput. Appl. Math.* **2011**, *235*, 1914–1924. [CrossRef]
4. Ali, E.H.; Ebaid, A.; Rach, R. Advances in the Adomian decomposition method for solving two-point nonlinear boundary value problems with Neumann boundary conditions. *Comput. Math. Appl.* **2012**, *63*, 1056–1065. [CrossRef]
5. Chun, C.; Ebaid, A.; Lee, M.; Aly, E.H. An approach for solving singular two point boundary value problems: Analytical and numerical treatment. *ANZIAM J.* **2012**, *53*, 21–43. [CrossRef]
6. Ebaid, A.; Aljoufi, M.D.; Wazwaz, A.-M. An advanced study on the solution of nanofluid flow problems via Adomian's method. *Appl. Math. Lett.* **2015**, *46*, 117–122. [CrossRef]
7. Bhalekar, S.; Patade, J. An analytical solution of fishers equation using decomposition Method. *Am. J. Comput. Appl. Math.* **2016**, *6*, 123–127.
8. Alshaery, A.; Ebaid, A. Accurate analytical periodic solution of the elliptical Kepler equation using the Adomian decomposition method. *Acta Astronaut.* **2017**, *140*, 27–33. [CrossRef]
9. Bakodah, H.O.; Ebaid, A. Exact solution of Ambartsumian delay differential equation and comparison with Daftardar-Gejji and Jafari approximate method. *Mathematics* **2018**, *6*, 331. [CrossRef]
10. Ebaid, A.; Al-Enazi, A.; Albalawi, B.Z.; Aljoufi, M.D. Accurate approximate solution of Ambartsumian delay differential equation via decomposition method. *Math. Comput. Appl.* **2019**, *24*, 7. [CrossRef]
11. Alenazy, A.H.S.; Ebaid, A.; Algehyne, E.A.; Al-Jeaid, H.K. Advanced Study on the Delay Differential Equation $y'(t) = ay(t) + by(ct)$. *Mathematics* **2022**, *10*, 4302. [CrossRef]
12. Ebaid, A. Remarks on the homotopy perturbation method for the peristaltic flow of Jeffrey fluid with nano-particles in an asymmetric channel. *Comput. Math. Appl.* **2014**, *68*, 77–85. [CrossRef]
13. Nadeem, M.; Li, F. He–Laplace method for nonlinear vibration systems and nonlinear wave equations. *J. Low Freq. Noise. Vib. Act. Control.* **2019**, *38*, 1060–1074. [CrossRef]
14. Ebaid, A.; Aljohani, A.F.; Aly, E.H. Homotopy perturbation method for peristaltic motion of gold-blood nanofluid with heat source. *Int. J. Numer. Meth. Heat Fluid Flow* **2020**, *30*, 3121–3138. [CrossRef]
15. Nadeem, M.; Edalatpanah, S.A.; Mahariq, I.; Aly, W.H.F. Analytical view of nonlinear delay differential equations using Sawi iterative scheme. *Symmetry* **2022**, *14*, 2430. [CrossRef]
16. Liao, S. *Beyond Perturbation: Introduction to the Homotopy Analysis Method*; CRC Press: Boca Raton, FL, USA, 2003.
17. Chauhan, A.; Arora, R. Application of homotopy analysis method (HAM) to the non-linear KdV equations Astha Chauhan and Rajan Arora. *Commun. Math.* **2023**, *31*, 205–220. [CrossRef]
18. Ebaid, A. Approximate periodic solutions for the non-linear relativistic harmonic oscillator via differential transformation method. *Commun. Nonlinear Sci. Numer. Simul.* **2010**, *15*, 1921–1927. [CrossRef]

19. Ebaid, A. A reliable aftertreatment for improving the differential transformation method and its application to nonlinear oscillators with fractional nonlinearities. *Commun. Nonlinear Sci. Numer. Simul.* **2011**, *16*, 528–536. [CrossRef]
20. Liu, Y.; Sun, K. Solving power system differential algebraic equations using differential transformation. *IEEE Trans. Power Syst.* **2020**, *35*, 2289–2299. [CrossRef]
21. Benhammouda, B. The differential transform method as an effective tool to solve implicit Hessenberg index-3 differential-algebraic equations. *J. Math.* **2023**, *2023*, 3620870. [CrossRef]
22. Abajo, J.G.D. Simple mathematics on COVID-19 expansion. *MedRxiv* **2020**. [CrossRef]
23. Gepreel, K.A.; Mohamed, M.S.; Alotaibi, H.; Mahdy, A.M.S. Dynamical behaviors of nonlinear coronavirus (COVID-19) model with numerical studies. *Comput. Mater. Contin.* **2021**, *67*, 675–686. [CrossRef]